VISION-BASED TRACKING SYSTEM FOR HEAD MOTION CORRECTION IN FMRI IMAGES

Tali Lerner and Ehud Rivlin
Department of Computer Science, Technion-Israel Institute of Technology, Haifa 32000, Israel

Moshe Gur
Department of Biomedical Engineering, Technion-Israel Institute of Technology, Haifa 32000, Israel

Keywords: fMRI, pose estimation, motion correction, tracking.

Abstract: This paper presents a new vision-based system for motion correction in functional-MRI experiments. fMRI is a popular technique for studying brain functionality by utilizing MRI technology. In an fMRI experiment a subject is required to perform a task while his brain is scanned by an MRI scanner. In order to achieve a high quality analysis the fMRI slices should be aligned. Hence, the subject is requested to avoid head movements during the entire experiment. However, due to the long duration of such experiments head motion is practically unavoidable. Most of the previous work in this field addresses this problem by extracting the head motion parameters from the acquired MRI data. Therefore, these works are limited to relatively small movements and may confuse head motion with brain activities. In the present work the head movements are detected by a system comprised of two cameras that monitor a specially designed device worn on the subject's head. The system does not depend on the acquired MRI data and therefore can overcome large head movements. Additionally, the system can be extended to cope with inter-block motion and can be integrated into the MRI scanner for real-time updates of the scan-planes. The performance of the proposed system was tested in a laboratory environment and in fMRI experiments. It was found that high accuracy is obtained even when facing large head movements.

1 INTRODUCTION

Magnetic Resonance Imaging (MRI) technology plays a central part in human brain research in the last decade (Belliveau et al., 1991; Bandettini et al., 1992). The utilization of MRI for brain functionality studies is referred to as *functional MRI* (fMRI). In fMRI studies a subject is requested to perform a task while his brain is repeatedly scanned. These tasks may include viewing images, listening to different sounds, performing a mathematical calculation and others. Statistical techniques are applied on the acquired fMRI scans in order to analyze the functionality of the examined parts in the subject's brain. The duration of an fMRI experiment may be relatively long (tens of minutes). During this time the subject is requested to avoid head movements in order to acquire aligning MRI scans along the experiment. The subject's head is stabilized (with pads) to prevent large head movements. However, small perturbations and slow drift of the head position are practically unavoidable. These motions deteriorate the alignment of scans that were acquired at different time instances, and therefore reduce the credibility and the accuracy of the statistical analysis (see Fig. 1). It is desirable to correct these displacement effects in the MRI slices before analyzing them.

The problem of motion correction in fMRI slices is discussed in several previous studies. Most studies derive the motion parameters from the acquired slices using different methods. These image-based techniques tend to fail in the presence of relatively large displacement. Additionally, due to brain activities, the gray levels of the image vary and may be confused with the head motion effects leading to a reduction in the accuracy of the motion estimates. Some of these studies handle 2D displacement in each slice separately and overlook the 3D nature of the head movement. Other studies extract the 3D motion parameters from the MRI slices under the assumption that no motion had occurred during the *block* (a set of subsequent MRI slices) acquisition but rather only between the different blocks.

The most traditional approach for finding the motion parameters is to compute the 2D transformation which best aligns a shifted image with a reference im-

Lerner T., Rivlin E. and Gur M. (2006).
VISION-BASED TRACKING SYSTEM FOR HEAD MOTION CORRECTION IN FMRI IMAGES.
In *Proceedings of the First International Conference on Computer Vision Theory and Applications*, pages 213-220
DOI: 10.5220/0001370202130220

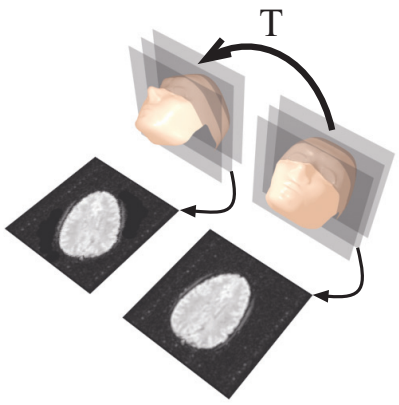

Figure 1: Illustration of the slice misalignment caused by the head motion. The acquired slices after the motion do not align with the original slices.

Figure 2: The system configuration. The subject is wearing the device on his head and the two cameras monitor the movements of the tracking device.

age. The alignment techniques can be classified into two groups: image intensity based and Fourier space based. The image intensity based group includes the works (Woods et al., 1992; Woods et al., 1993) which suggest defining images as being effectively the same when their voxel-by-voxel ratio is a constant. (Hajnal et al., 1995) suggests defining the difference between images using the mean square voxel-by-voxel error. Other intensity based works can be found in (Friston et al., 1996; Thesen et al., 2000; Ciulla and Deek, 2002). The Fourier space alignment techniques detect the motion parameters using Fourier methods that can be applied on the raw data of MRI images since it is collected in that domain. Examples of such techniques can be found in (Zoroofi et al., 1996; Kim et al., 2002; Caparelli et al., 2003). A different approach can be found in (Derbyshire et al., 1998). The described real-time system extracts the 3D position of the subject's head from an external source of information. Three coils are attached to the subject's head and their spacial location is monitored using magnetic resonance techniques. The computed motion is applied on the MRI scan-plane in order to chase the subject's head. The disadvantage of this system is the limited number of features (the coils) that lead to poor estimation of head position.

In the present work a new vision-based solution to the head motion correction problem is presented. The proposed system includes two calibrated and synchronized cameras for tracking the movements of a specially designed device which is worn on the subject's head. The monitored motion is utilized to produce motion-free MRI slices. Similarly to (Derbyshire et al., 1998) the system computes the 3D motion parameters using an external source of information (the optical tracking configuration), and therefore it can overcome extremely large head motion. Although the system presented here assumes no head motion during the block acquisition it can be easily extended to cope with inter-block motion when detecting the head position for each slice separately.

The rest of this paper is organized as follows: Section 2 gives a brief overview of the system. Section 3 describes the algorithms and devices used for the system calibration. The algorithms and devices used for the motion detection are described in Section 4. A method for correcting the MRI data is presented in Section 5. Section 6 elaborates on a series of lab experiments and Section 7 shows qualitative and quantitative results when applying the system in a real fMRI experiment. Finally, conclusions are noted in Section 8.

2 SYSTEM OVERVIEW

The system presented in this work is composed of a specially designed tracking device which is strapped to the subject's head, and two cameras with zooming capability. The cameras are positioned on both sides of the MRI bed and monitor the movements of the tracking device (see Fig. 2). When using the system, three main stages are performed: system calibration, head motion detection, and MRI blocks correction.

In the system calibration stage, the internal parameters of the two cameras and their relative position are computed. Once this information is evaluated the *pose* (position + orientation) of the subject's head w.r.t the cameras' coordinate systems can be accurately detected using stereopsis methods. Since the final objective is to correct the motion in the MRI slices, the head motion w.r.t the MRI system is required. For that aim the pose of the cameras w.r.t the MRI system is also extracted during the calibration phase.

Once the system is calibrated the fMRI experiment

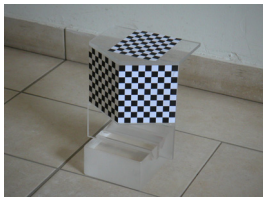

Figure 3: The calibration device designed for computing the relative position of the cameras.

(a) (b)

Figure 4: The phantom device designed for linking the cameras to the MRI coordinate system.

can begin. A head device is strapped to the subject's head during the experiment. Due to rigid body motion laws a single motion transformation applies to both the head and the head device. Therefore, by monitoring the pose of the head device the head movements can be deduced. Using the cameras relative position w.r.t the MRI, the head motion transformation can be expressed under the MRI coordinate system.

Finally, the MRI blocks can be corrected. Utilizing the head motion transformation, a compensating transformation can be applied on the MRI blocks. The generated motion-free blocks are the blocks that would have been obtained in the absence of head motion.

3 SYSTEM CALIBRATION

The calibration procedure starts by obtaining the internal parameters of each camera using a standard technique (Bouguet,). Next, the relative pose between the two cameras and their pose w.r.t the MRI system are estimated. The rest of this section elaborates on the methods and the custom made devices that participate in these procedures.

3.1 Finding the Cameras Relative Position

Extremely accurate pose estimates are required for a qualitative motion correction of the fMRI slices. For this purpose, a multi-camera pose estimation algorithm, referred to as *TwoCamPose*, is presented in Section 4.2. This algorithm requires the relative position and orientation between the two cameras. The accuracy of this connecting transformation significantly influences the obtained accuracies of the TwoCamPose algorithm. A calibration device composed of three planes is designed. Two planes create an angle of 120° and the third plane is orthogonal to both of them. On each plane a chessboard image was attached (see Fig. 3). The 3D locations of the corners on the three chessboards are known and serve as features for the device pose computation. The fact that the features constellation is not coplanar drastically improves the accuracy of the obtained pose estimates. The device is placed in several positions and its poses w.r.t each of the cameras are computed. The connecting transformation between the cameras is computed as the composition of the device poses:

$$ {}^{cam2}_{cam1}T = {}^{cam2}_{device}T \cdot {}^{device}_{cam1}T \qquad (1) $$

where ${}^{B}_{A}T$ represents the Euclidean transformation from coordinate system A to B. The parameters of these composed transformations are averaged to derive the final estimate of the cameras relative position and orientation.

3.2 Cameras Pose w.r.t the MRI Coordinate System

Although the cameras' relative position enables the computation of the tracking device pose w.r.t the cameras, the required information is its motion w.r.t the MRI coordinate system. Therefore, the linking transformation from the cameras coordinate system to the MRI coordinate system is necessary. For this purpose a device, referred to as *phantom*, is designed (see Fig. 4(b)). This device is composed of two main components. At the front end a planar chessboard is installed. Using the TwoCamPose algorithm the pose of the phantom device is obtained. At the back end, a $120 \times 120 \times 50$ mm water container is attached see Fig. 4(a). This container is scanned by the MRI scanner using high resolution parameters. Next, the slices produced by the MRI scanner are registered to the geometrical model of the container. In order to acquire the 3D registration parameters with high accuracy, sixteen stakes were added to the geometrical structure of the container. Once the poses of the phantom w.r.t the MRI system and the cameras are known, the linking transformation between the cameras and the MRI system is derived.

Figure 5: The head device strapped to a subject's head.

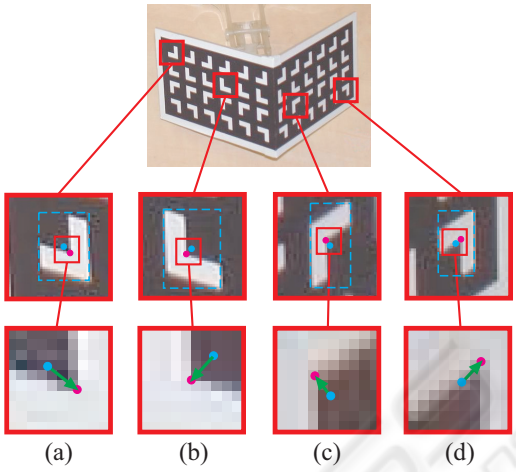

Figure 6: Orientation classification method of the L-shaped features on the tracking device. The cyan dot represents the center of the feature's bounding box while the purple dot represents its center of gravity. The classification method utilizes the direction of the green arrows shown in (a)-(d).

4 MOTION DETECTION

This section details the heart of the system that is presented in this paper. The detection of the subject's head motion is performed throughout the entire fMRI experiment. A specially designed device is strapped to the subject's head and is monitored by the two cameras. Later, the recorded information is analyzed in order to compute the compensating transformations for the MRI slices.

4.1 The Head Device

Monitoring the head movements is performed using a device that is worn by the subject. The device is composed of a strip which is placed on the subject's head, and two rods attached to it from both sides of the head near his temples. These rods are linked together in front of the chin to a *tracking device* that is monitored by the cameras (see Fig. 5). The tracking device is built of two 50×80 mm planes that create an angle of 90° between them. "L"-shaped features are arranged in four rows on the tracking device planes. The features in each row have a unique orientation which assist in the correspondence solution. The features orientation is detected by examining the direction of the vector from the center of the L-feature bounding-box to its gravity-center (see Fig. 6). The described configuration of the tracking device enables obtaining the head motion with high accuracy, as can be observed in Section 6.

4.2 The "TwoCamPose" Algorithm

During the system calibration procedure the relative position of the two cameras is computed. Utilizing this piece of information, the pose of the tracking device can be obtained in a straightforward manner: first, the 3D location of each feature is separately reconstructed w.r.t the cameras using a standard triangulation algorithm (Hartley and Zisserman, 2000). Next, the pose is computed from the 3D-to-3D feature registration (Umeyama, 1991). This approach is advantageous because both steps have closed-form solutions which make them computationally attractive. However, the triangulation step of the above approach overlooks the known 3D constellation of the features. Since the pose estimation computation is performed off-line, obtaining high accuracy is preferred over computational duration. Hence, an alternative method for the pose computation, referred to as "*TwoCamPose*", is proposed. Let p_i be the 3D location of the i'th feature w.r.t the coordinate system of the model. Let t_{12} and R_{12} be the relative position and orientation, respectively, between the two cameras. Given the 2D measurements from each of the cameras - $\tilde{I}_{i,1}$ and $\tilde{I}_{i,2}$, this algorithm searches for the pose that minimizes the objective-function:

$$\sum_{i=1}^{n} \left(\frac{v_i}{(v_i)_z} - \tilde{I}_{i,1} \right)^2 + \left(\frac{R_{12}v_i + t_{12}}{(R_{12}v_i + t_{12})_z} - \tilde{I}_{i,2} \right)^2, \quad (2)$$

where $v_i = R \cdot p_i + t$, R and t are the pose hypothesis. The above function reflects the sum of the squared distances between the 2D extracted features from each camera and their reprojected 3D features given a pose hypothesis. This function was minimized using the Newton-Raphson optimization technique. Although the TwoCamPose algorithm is presented for only two cameras it can be easily extended to an arbitrary number of cameras. The TwoCamPose algorithm achieves more accurate pose estimates than the triangulation technique as will be shown in Section 6.

4.3 Construction of the Compensating Transformation

By composing two poses of the tracking device w.r.t the cameras, the device's motion, and thus the subject's head motion, is computed. Therefore, this motion transformation is also obtained w.r.t the cameras. Since the fMRI slices are acquired w.r.t the MRI system, the motion transformation must be expressed w.r.t the same system. Consider two time instances: t_0 and t_1, before and after a single movement of the head. Each time instance corresponds to a coordinate system D_0 and D_1 attached to the tracking device. Consider a point p_0 in the subject's brain. Due to the head movement this point is transferred to a new position p_1. Since it is assumed that the tracking device and the head move rigidly:

$$^{D_0}p_0 = {}^{D_1}p_1. \tag{3}$$

In the above equation the left superscript describes the coordinate system in which the vector is represented. Let $\tilde{T}$ be the desired transformation between the points p_0 and p_1 under the MRI coordinate system. Using this transformation one can write:

$$^{MRI}p_1 = \tilde{T} \cdot {}^{MRI}p_0. \tag{4}$$

The positions of p_0 and p_1 in the MRI system are given by

$$^{MRI}p_i = {}^{MRI}_{D_i}T \cdot {}^{D_i}p_i \tag{5}$$

where $i = 1, 2$. Assigning Equation (5) to both sides of Equation (4) yields:

$${}^{MRI}_{D_1}T \cdot {}^{D_1}p_1 = \tilde{T} \cdot {}^{MRI}_{D_0}T \cdot {}^{D_0}p_0. \tag{6}$$

Multiplying the left side of (6) by ${}^{D_1}_{MRI}T$ results:

$$^{D_1}p_1 = {}^{D_1}_{MRI}T \cdot \tilde{T} \cdot {}^{MRI}_{D_0}T \cdot {}^{D_0}p_0. \tag{7}$$

Recalling (3), the multiplication of the three transformations must be the identity transformation I:

$${}^{D_1}_{MRI}T \cdot \tilde{T} \cdot {}^{MRI}_{D_0}T = I. \tag{8}$$

Multiplying by the inverse transformations yields the final result:

$$\tilde{T} = {}^{MRI}_{D_1}T \cdot {}^{D_0}_{MRI}T. \tag{9}$$

This transformation supplies a description of the subject's head motion between two time instances during the fMRI experiment.

In this work the first block is perceived as the reference block while the rest of the blocks are corrected according to its position. As a result, the movements between the reference block and the rest of the blocks w.r.t the MRI coordinate system are computed as described above. Similarly to (Derbyshire et al., 1998) the $\tilde{T}$ transformation could be supplied to the MRI scanner in order to update the scan-planes position. This way the slices chase the subject's head position during their acquisition and therefore no postprocessing motion compensation is necessary.

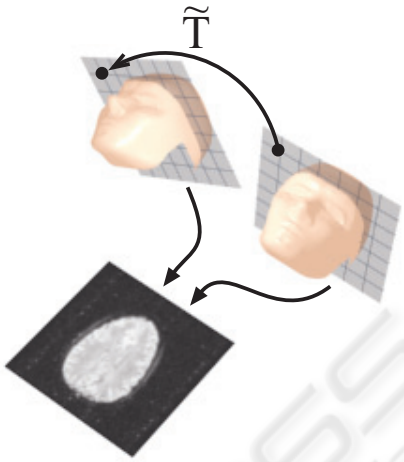

Figure 7: Motion compensation in the fMRI slices. The head movement transformation – $\tilde{T}$ is applied to each of the MRI slices' grid points.

5 MOTION COMPENSATION IN MRI SLICES

The motion compensation is the final step of the system presented in this work. In this step, motion-free slices are synthesized from the existing MRI slices using the head movement transformation - $\tilde{T}$. As mentioned above, a single transformation is assigned to each block in the fMRI data. By applying this transformation on the block, its slices chase the subject's moving head. Each slice is represented by a 3D regular and planar grid. The grid points represent the center of voxels in the MRI scan. The location of the grid points w.r.t the MRI coordinate system is supplied by the MRI image format. In order to produce the motion-free slice, the $\tilde{T}$ transformation is applied on each of the grid points (see Fig. 7). The new gray level of the transformed grid point is determined by identifying its eight surrounding voxels in the origin block and applying trilinear interpolation on their gray level values.

6 LAB EXPERIMENTS

A series of lab experiments were conducted to evaluate the ability of the TwoCamPose algorithm described in section 4.2 to detect small motions and compare its accuracy to the triangulation based 3D reconstruction algorithm described in the same section. The tracking device was attached to a robotic arm and small motion was applied to it. The experiment involved moving the tracking device along

a constant direction by ten steps of 0.1 mm in order to complete a trajectory of 1 mm. The motion was translational only, no rotation was involved. The eleven poses were estimated using the two evaluated algorithms. Although the structure of the true trajectory was known (pure translational motion along a constant direction), its relative position w.r.t the cameras was unknown. In order to overcome this obstacle, least squares alignment was performed between the true trajectory and the measured trajectory (the eleven poses), and the distances between the two fitted trajectories were measured. Three different trajectories were examined. Each one aligned with one of the main axes: X, Y, and Z. Tables 1 and 2 compare the mean and maximal errors of the two evaluated algorithms computed from the three trajectories. One can easily observe that the TwoCamPose algorithm achieves better results. The results of the experiment indicate that motions as small as 0.1 mm can be detected with high accuracy using the TwoCamPose algorithm. These accuracies are very small compared to the fMRI image resolution which is at least 1.75 mm in X and Y axes and 2.8 mm in the Z axis.

7 RESULTS

In this section the results that were obtained by the system described in this work are presented. fMRI experiments with a subject were conducted. The subject wore the head device and visual stimulations were presented to him while his brain was scanned (see Fig. 2 for the experiment's setup). Three experiments were recorded. In the first one the subject was asked to avoid motion as much as possible, in the second experiment the subject was asked to move slightly; and in the last experiment the subject was allowed to perform larger movements.

The algorithms described in this work were applied on the recorded MRI blocks producing new motion-free blocks. These corrected blocks were compared to the original (uncorrected) blocks both qualitatively and quantitatively. Figures 8 through 10 show an example of the displacement and the correction quality of a single slice. In each figure, the blue line represents the contour of the brain in the first block, the red dashed line represents the contour of the brain taken from another block, and the green dashed line represents the contour of the brain taken from the same block after compensation. As can be observed, the brain offset was correctly detected and compensated even in cases of large head motion. In Fig. 11 the average image of the corresponding slices taken from all the original blocks is compared to the same one taken from the corrected blocks. As can be observed, the average image of the original blocks is blurred and

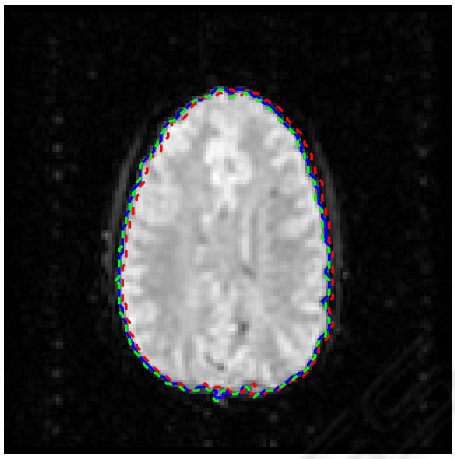

Figure 8: Motion compensation in a slice from the first experiment (no intended motion).

unclear while these artifacts are significantly reduced in its corrected counterpart.

In addition to the described qualitative results, a quantitative comparison between the original and the corrected blocks from the three experiments is presented in Table 3. Two measurements were used for this comparison: correlation coefficient and Forbenius norm. The correlation coefficient is computed by:

$$c = \frac{\sum_m \sum_n (R_{mn} - \bar{R})(A_{mn} - \bar{A})}{\sqrt{(\sum_m \sum_n (R_{mn} - \bar{R})^2)(\sum_m \sum_n (A_{mn} - \bar{A})^2)}} \quad (10)$$

where A is a slice and R is its corresponding reference slice. $\bar{R}$ and $\bar{A}$ are the mean values of the these slices. The Forbenius norm value is defined as:

$$f = \sqrt{\sum_m \sum_n (R_{mn} - A_{mn})^2}. \quad (11)$$

For both measurements the first block served as a reference block. The similarity between each slice and its corresponding slice in the reference block was evaluated by the two measurements. The similarity of the entire experiment was evaluated by averaging the similarity measurement of all its slices. As shown in Table 3 the alignment quality of the original blocks deteriorates when the motion's magnitude increases. The corrected blocks, on the other hand, maintain high and almost constant alignment quality for all motion types. These results verify the advantage of utilizing the proposed system in fMRI experiments.

Table 1: Comparison of the translation errors in each trajectory between the TwoCamPose and the Triangulation algorithms described in Section 4.2. The translation error is measured in mm.

Alg.	X		Y		Z	
	Mean	Max	Mean	Max	Mean	Max
TwoCamPose	0.0204	0.0335	0.0277	0.0721	0.0283	0.0559
Triangulation	0.0651	0.1308	0.0719	0.186	0.0602	0.1055

Table 2: Comparison of the rotation errors in each trajectory between the TwoCamPose and the Triangulation algorithms described in Section 4.2. The angular error is measured in degrees.

Alg.	ϕ		θ		ψ	
	Mean	Max	Mean	Max	Mean	Max
TwoCamPose	0.0131	0.0197	0.0117	0.017	0.0115	0.0162
Triangulation	0.0801	0.1734	0.0619	0.1418	0.0736	0.1195

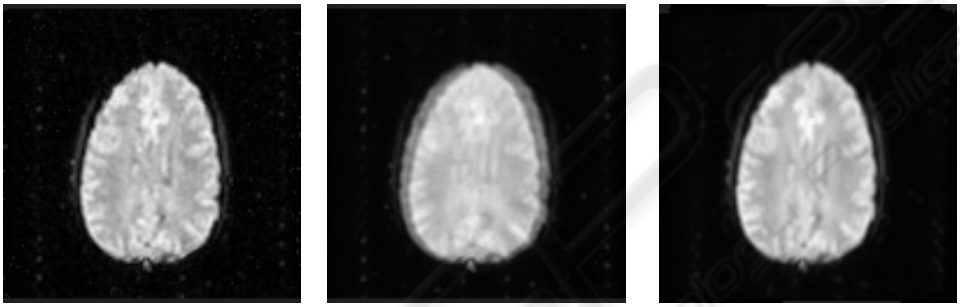

(a) (b) (c)

Figure 11: Average images comparison of the third experiment (relatively large intended motion). (a) a slice from the first (reference) block. (b) the average image of the corresponding slices from all the original blocks. (c) the average image of the corresponding slices from all the corrected blocks.

Table 3: In this table the original and corrected blocks are compared by the average correlation coefficient (Equation 10) and average Forbenius norm (Equation 11) which were obtained from the three experiments.

	Small Motion		Medium Motion		Large Motion	
	Correlation	Forbenius	Correlation	Forbenius	Correlation	Forbenius
Original	0.9865	6.1136	0.9816	7.3265	0.9411	13.569
Corrected	0.9963	3.8939	0.9957	3.8394	0.9946	4.3644

8 CONCLUSIONS

In this paper a new vision-based system for motion correction in fMRI experiments is proposed. The quality of the experiment's analysis significantly depends on the magnitude of the subject's head movements while the MRI scans were acquired. Due to the typical long duration of an fMRI experiment, head motion is practically unavoidable. Most of the previous work in this field addressed this problem by extracting the head motion parameters from the acquired MRI data. The system that was presented here detects the head movements using two calibrated cameras that monitor a head-device worn by the subject during the experiment. The system does not depend on the acquired MRI data and therefore can overcome large head movements. Additionally, the system can be extended to cope with inter-block motion and can be integrated into the MRI scanner for real-time updates of the scan-planes. As was shown in the lab experiments, the head motion is detected with sub-millimetric accuracy. The applicability of the system was tested with subjects and proved to achieve a high quality correction of corrupted MRI data even when dealing with large head motion.

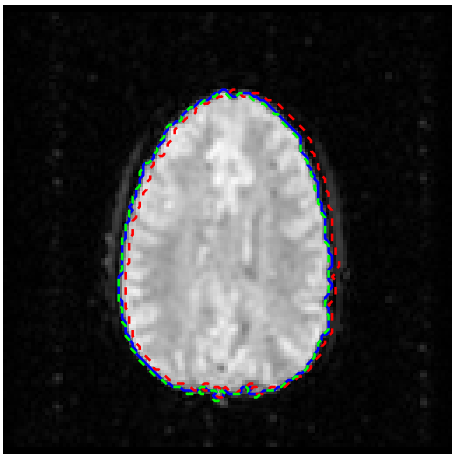

Figure 9: Motion compensation in a slice from the second experiment (small intended motion).

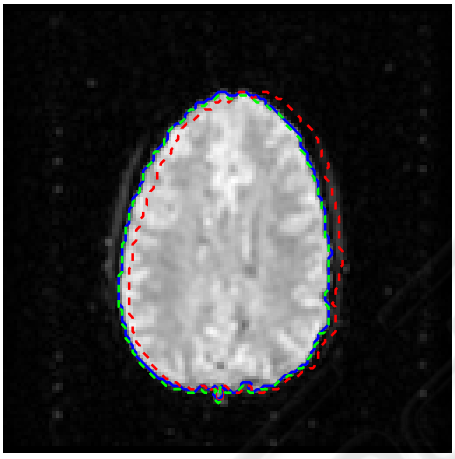

Figure 10: Motion compensation in a slice from the third experiment (relatively large intended motion).

REFERENCES

Bandettini, P., Wong, E., Hinks, R., Tikofsky, R., and Hyde, J. (1992). Time course epi of human brain function during task activation. *Journal of Magn. Reson. Med.*, 25:390–397.

Belliveau, J., Kennedy, D., McKinstry, R., Buchbinder, B., Weisskoff, R., Cohen, M., Vevea, J., Brady, T., and Rosen, B. (1991). Functional mapping of the human visual cortex by magnetic resonance imaging. *Science*, 254:716–719.

Bouguet, J. Camera calibration toolbox for matlab. www.vision.caltech.edu/bouguetj/calib_doc.

Caparelli, E., Tomasi, D., Arnold, S., Chang, L., and Ernst, T. (2003). K-spaced based summary motion detection for functional magnetic resonance imaging. *NeuroImage*, 20:1411–1418.

Ciulla, C. and Deek, F. (2002). Performance assessment of an algorithm for the alignment of fmri time series. *Brain Tomography*, 14:NO. 4.

Derbyshire, J., Wright, G., Henkelman, R., and Hinks, R. (1998). Dynamic scan-plane tracking using mr position monitoring. *Journal of Magn. Reson. Med.*, 5:924–932.

Friston, K., William, S., Howard, R., Frackowiak, R., and Tuner, R. (1996). Movement-related effects in fmri time-series. *Journal of Magn. Reson. Med.*, 35:346–355.

Hajnal, J., Saeed, N., Soar, E., Oatridge, A., Young, I., and Bydder, G. (1995). A registration and interpolation procedure for subvoxel matching of serially acquired mr images. *Journal of Computer Assisted Tomography*, 19:289–296.

Hartley, R. and Zisserman, A. (2000). *Multiple View Geometry in Computer Vision*. Cambridge University Press, Cambridge.

Kim, E., Park, N., Choi, M., and Tamura, S. (2002). Cancellation of mri motion artifact in image plane. In *IEEE Intrumentation and Measurements*.

Thesen, S., Hied, O., Mueller, E., and Schad, L. (2000). Prospective acquisition correction for head tracking for real-time fmri. *Journal of Magn. Reson. Med.*, 44:457–465.

Umeyama, S. (1991). Least-squares estimation of transformation parameters between two point patterns. *IEEE Trans. on Pattern Analysis and Machine Intelligence*, 13,Journal of Computer Assisted Tomography:376–380.

Woods, R., Cherry, S., and Mazziotta, J. (1992). Rapid automated algorithm for aligning and reslicing pet images. *Journal of Computer Assisted Tomography*, 16:620–633.

Woods, R., Mazziotta, J., and Cherry, S. (1993). Mri-pet registration with automated algorithm. *Journal of Computer Assisted Tomography*, 17:536–546.

Zoroofi, R., Sato, Y., S.Tamura, and Naito, H. (1996). Mri artifacts cancellation due to rigid motion in the imaging plane. *IEEE Tran. on Medical Imaging*, 15:NO. 6.